Phase Analysis of the Stretching Cycles of the Head of Unsteady Gravity Currents Developing over Smooth and Rough Beds

Helena I. S. Nogueira
Ph.D. Student, Dept. Civil Eng. & IMAR-CMA, University Coimbra, Coimbra, Portugal. Email: hnogueira@dec.uc.pt

Claudia Adduce
Assistant Professor, Dept. Civil Eng., University of Roma Tre, Rome, Italy. Email: adduce@uniroma3.it

Elsa Alves
Research Officer, Hydraulics and Environment Department, National Laboratory of Civil Engineering, Lisbon, Portugal. Email: ealves@lnec.pt

Mário J. Franca
Research and Teaching Associate, Laboratory of Hydraulic Constructions, École Polytechnique Fédérale de Lausanne, Lausanne, Switzerland. E-mail: mario.franca@epfl.ch

ABSTRACT: Gravity currents are buoyancy driven flows occurring spontaneously in nature or resulting from human intervention. Examples of gravity currents in the water are oceanic fronts, resulting from differences in temperature and salinity, and turbidity currents caused by high concentration of suspended particles. The release of pollutant materials into rivers, oil spillage in the ocean and desalination plant outflows are examples of anthropogenic gravity currents in the water, frequently with negative environmental impacts. The present work experimentally investigates the dynamics of unsteady gravity currents produced by lock-release of a saline mixture into a fresh water tank. Seven different experimental runs were performed by varying the density of the saline mixture in the lock and the bed roughness. The experiments were conducted in a 3.0 m long Perspex flume, of horizontal bed and rectangular cross section of 0.20 x 0.30 m^2, and recorded with a 25 Hz CCD video camera. An image analysis technique was applied to visualize and characterize the current allowing the detailed analysis of the gravity current dynamics and more specifically of the head dynamics. The temporal evolution of variables assessed at the head of the gravity current i.e. length, surface, volume and mass, per unit width, shows repeated cycles of stretching and break of the head. During the stretching phase, ambient fluid is entrained into the head causing its growth. However this is not unlimited, a limit in which the head becomes unstable and consequently breaks exists. There is a strong similarity in the head aspect ratio, of maximum head height to length, and mass between the cycles and between runs, thus a phase lumped analysis within the periodically well-behaved cycles is presented in terms of head aspect ratio, head mass and mass rate. In the instants of head break, the head aspect ratio shows a consistent limit of 0.2, for all runs, and the mass of the head is of the order of the initial mass in the lock. Regarding the periodicity of the break events, it is seen to increase with bed roughness. Entrainment at the head is evaluated through mass rate and is seen to occur during all the stages of the current development.

KEY WORDS: Gravity Currents, Lock-Exchange, Image Analysis Technique, Entrainment.

1 INTRODUCTION

Gravity or density currents are flows driven by buoyancy occurring spontaneously in nature or as a result of human intervention. Examples of gravity currents in the atmosphere are sea-breeze fronts, driven by differences in temperature between two air masses, and avalanches of airborne snow and sand storms, where suspended particles play a major role in density gradients. In the water masses one may refer oceanic fronts, resulting from differences in temperature and salinity, and turbidity currents caused by high concentration of suspended particles. Several more examples can be found comprehensively in Simpson (1997).

Gravity currents are pertinent to engineering sciences, namely in what concerns industrial safety and

environmental protection. The release of pollutant materials into rivers, oil spillage in the ocean and desalination plant outflows are a few examples of anthropogenic gravity currents frequently with negative environmental impacts. The loss of storage in reservoirs related to the deposition of fine sediments transported by turbidity currents, gravity currents where density difference is given by fine suspended sediments, is a subject of great concern to hydraulic engineers.

In the last 30 years advances have been made on the analysis of the physics of density currents, both by using experimental (Rottman and Simpson 1983, Hacker et al. 1996, Marino et al. 2005) and numerical modeling (Härtel et al. 2000, Ooi et al. 2007, Paik et al. 2009, Bombardelli et al. 2009). Several studies have been developed through image analysis technique to investigate the dynamics of gravity currents (Adduce et al. 2009, La Rocca et al. 2008); the present research, based on experimental work, uses similar techniques (Nogueira et al. 2013a and Nogueira et al. 2013b).

Here we investigate the dynamics of the head region of gravity currents performed by lock-exchange releases of saline water into a fresh water tank. Seven different lock-exchange tests were performed varying the initial density of the saline mixture and the bed roughness. Stretching periods followed by break were previously observed in the current head (preliminary described in Nogueira et al. 2012). These cycles are especially well evident when observing the time evolution of the head length, surface, volume and mass. A phase analysis is performed and applied to geometric and dynamic quantities evaluated at the head of the gravity currents, for all the experimental runs.

After this introduction, experimental details are given in section 2, main results concerning the periodic cycles are presented and discussed in section 3, being section 4 devoted to the main conclusions.

2 EXPERIMENTAL DETAILS

The experiments were carried out at the Hydraulics Laboratory of University Roma Tre, in a 3.0 m long transparent Perspex tank with a 0.2 m wide and 0.3 m deep rectangular cross-section (Figure 1).

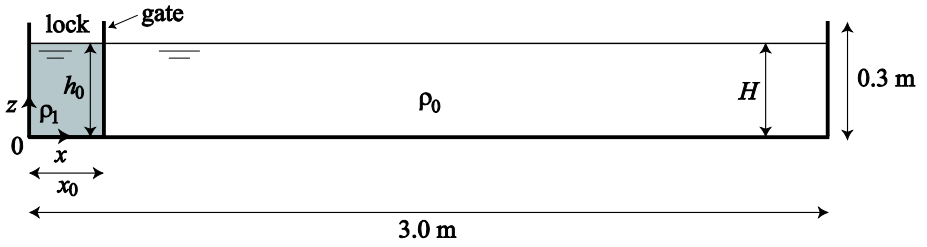

Figure 1 Schematic view of the Perspex tank aimed at the lock-exchange experiments with main dimensions and the Cartesian reference system considered

A vertical sliding gate is placed in the tank at a distance $x_0 = 0.15$ m from the left wall to form a lock. The right side of the tank is filled with fresh water with density ρ_0, whereas the lock is filled with saline mixture with density ρ_1; both sides filled up at same depth, $h_0 = 0.20$ m. A controlled quantity of white colorant is added to the mixture in the lock to provide flow visualization. The outside back wall of the tank is lined with black paperboard to produce a dark, uniform background to contrast with the white dyed developing gravity current.

At the beginning of each experiment the gate is suddenly removed, leaving the dense fluid to flow under the fresh water. A return current formed by ambient fluid develops above the denser current in the opposite direction. During this process, mixing between both currents takes place, inducing entrainment of ambient fluid into the heavier density current, reducing its density. The experiment ends when the current reaches the right end wall of the tank.

The evolution of the gravity current is recorded by a CCD video camera with 768 x 576 pixels of resolution and acquisition frequency of 25 Hz. The video frames are subsequently converted into gray scale matrices in the region of the tank with fluid and then converted into instantaneous density fields of the current through an adequate calibration procedure. In Nogueira et al. (2013a) and Nogueira et al. (2013b) further details on the experiments, calibration procedure and error analysis and correction may be

found.

Seven lock-exchange experiments were performed varying the initial density of the saline mixture in the lock, ρ_1, and the bed roughness, k_s, leading to two different types of runs: D and R, respectively. The experiments were performed by varying one parameter at a time. Table 1 summarizes the parameters of the experiments.

Table 1 Main parameters of the experimental runs

Run	ρ_0 (kgm^{-3})	ρ_1 (kgm^{-3})	k_s (mm)	g'_0 (ms^{-2})	u_0 (ms^{-1})	R_0 (-)	Symbols in figures
D1	997.8	1014.7	0.0	0.17	0.18	40756	○
D2	997.4	1029.7	0.0	0.32	0.25	53230	□
D3	997.4	1044.6	0.0	0.46	0.30	66918	△
D4	998.0	1060.0	0.0	0.61	0.35	64680	▽
R1	997.4	1030.0	2.9	0.32	0.25	64922	+
R2	997.4	1030.1	4.6	0.32	0.25	55058	x
R3	997.6	1030.2	24.6	0.32	0.25	52479	*

The initial reduced gravity acceleration, g'_0, is defined as:

$$g'_0 = g\frac{\rho_1 - \rho_0}{\rho_0} \tag{1}$$

in which g is the acceleration of gravity. The buoyancy velocity, u_0, is defined as:

$$u_0 = \sqrt{g'_0 h_0} \tag{2}$$

and R_o is a bulk Reynolds number defined as:

$$R_0 = \frac{u_0 h_0}{\nu} \tag{3}$$

where ν is the kinematic viscosity of the saline mixture, a function of temperature, pressure and concentration of salt and herein obtained through the results presented in Kestin et al. (1981). Bulk Reynolds number is always larger than 40000, indicating the turbulent nature of the gravity currents performed in this study.

Rough bed was made by placing a $3D_{50}$ thick layer of sediments, mainly constituted by quartz and feldspar, where D_{50} is the grain size diameter for which 50% of the amount of sediments has smaller diameters; herein D_{50} was taken as the roughness scale k_s. The tank was leveled horizontally and the grains were set uniformly throughout the tank, where no bed forms were allowed.

3 RESULTS

3.1 Head definition

The criterion used to characterize and isolate the head region was based on a dynamic function given by the product between local values of depth-averaged density, $\overline{\rho}_v$, and current height, h (cf. Nogueira et al. 2012, 2013b):

$$W(x,t) = \overline{\rho}_v(x,t)h(x,t) \tag{4}$$

The downstream limit of the head is given by the position of the foremost point of the current, being the upstream limit, and consequently the head length L_h, defined by taking the position of the first meaningful local minimum of function W, near the front.

Figure 2 shows the temporal evolution of the head length, L_h, plotted as a function of dimensionless time, tu_0/x_0, defined after the gate removal for all experiments.

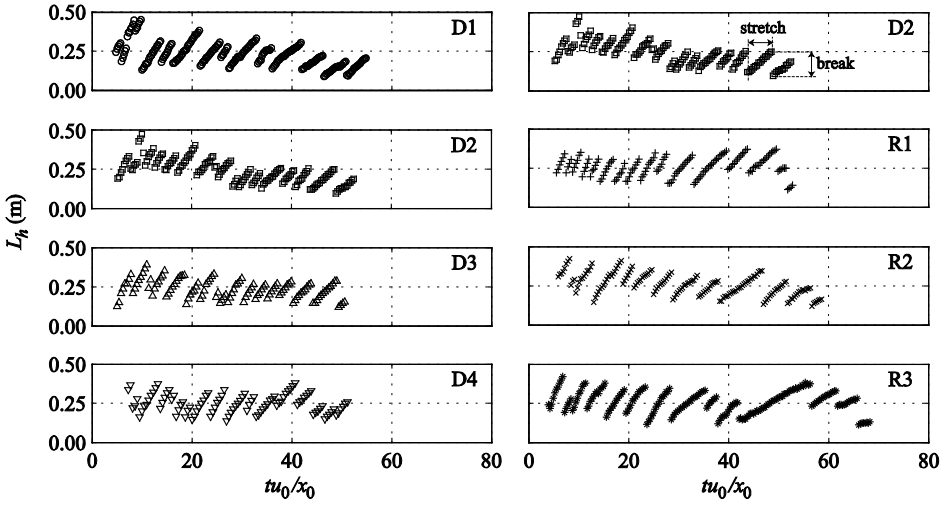

Figure 2 Length of the gravity current head, L_h, as a function of dimensionless time. Left: runs of series D, performed with smooth bed, k_s = 0, and increasing ρ_1; right: runs of series R, performed with fixed ρ_1 and increasing bed roughness.

Cyclic patterns characterized by successive events of stretching and break of the head are observed. Similar behavior was detected when analyzing other variables computed at the head, namely head surface, volume and mass, not presented here. During the stretching phase, a general increase of the head is observed due to entrainment of ambient fluid into the head region. Figure 2 shows a faster rate of increase of head length during the first phase of the current development, suggesting that entrainment at the head is present throughout its development, inclusively in the early stages. This observation is in agreement with the observations of Hacker et al. (1996), though deviating from the theory of Hallworth et al. (1996). The break cycles indicate that a limit exists in the entrainment capacity of the head.

3.2 Stretching cycles

Table 2 presents the average and maximum non-dimensional wavelength, $L^* = L/x_0$, where L is the spatial distance between front positions of two successive break events and the average and maximum non-dimensional period between break events, $T^* = Tu_0/x_0$, being T the time between two successive breaks.

Table 2 Average ($\bar{}$) and maximum ($_{max}$) normalized temporal (T) and spatial (L) periodicity of break events.

Run	$\overline{T}^*$	T^*_{max}	$\overline{L}^*$	L^*_{max}
D1	3.3	5.9	1.1	2.0
D2	2.5	5.2	0.9	1.5
D3	2.7	5.5	0.9	1.8
D4	2.6	4.2	0.9	1.6
R1	3.0	6.8	1.0	2.0
R2	4.1	8.8	1.3	2.3
R3	4.6	14.4	1.2	2.9

The analysis of the average and maximum values of T^* show a tendency between runs. Regarding the effect of the initial density for smooth bed (series D), we observe that run D1, with lower initial density, has the highest average and maximum stretching periods. A significant decrease in the average periodicity is observed from run D1 to D2, which apparently stabilizes with the following increase of initial density. The effect of bed roughness can be observed by analyzing the sequence D2, R1, R2 and R3.

The average period suggests that as the bed roughness increases, breaking events tend to occur less frequently and a temporal extension of the stretching phases occurs. A similar trend is observed when looking to the maximum period and maximum wavelength between break events: an increase is detected when increasing the bed roughness. The average wavelength is approximately constant between runs, $L^* = 1.1 \pm 0.2$.

The head aspect ratio of height to length, h_m/L_h, where h_m is the maximum height of the head during each cycle, is plotted in Figure 3 for all runs against the dimensionless front position defined as $(x_f - x_0)/x_0$, where $x_f(t)$ is the front position of the gravity current. The aspect ratio of the head is seen to decrease during the stretching period, which is expected since the maximum height of the head has little variation over time while the head length increases continuously during stretching.

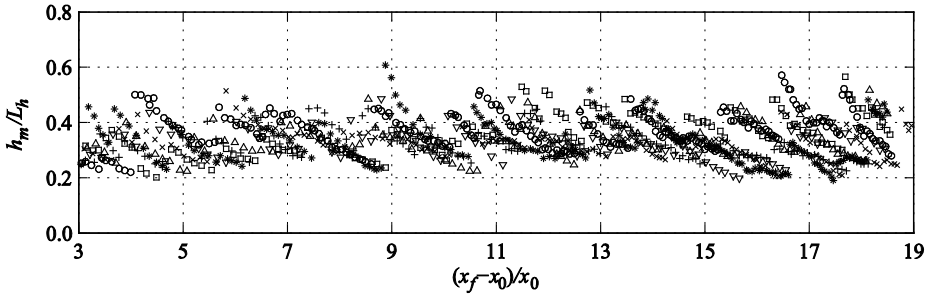

Figure 3 Head aspect ratio, h_m/L_h, as function of non-dimensional front position (symbols explained in Table 1).

A limit in the entrainment capacity of the head seems to exist for $h_m/L_h \approx 0.2$, lower data boundary in Figure 3. Britter and Linden (1980) argued that the head aspect ratio of constant-flux gravity currents developing over horizontal beds is zero. Özgökmen et al. (2004) present a limit of $h_m/L_h = 0.2$, for numerical modeling in lock-exchange gravity currents down slope (3.5°), being 0.25 their average or trend. Hence, the limit given by the head aspect ratio, $h_m/L_h \approx 0.2$, seems to be a good criterion to predict the instant of head breaking, for unsteady currents developing over horizontal beds, or even, over low slopes.

3.2 Phase analysis

A phase analysis is performed over one stretching cycle of duration θ, normalized from 0 to 1, where 0 is the beginning and 1 the end of the cycle. Figure 4 shows h_m/L_h data for run D1, phase-sampled over all stretching cycles and plotted together.

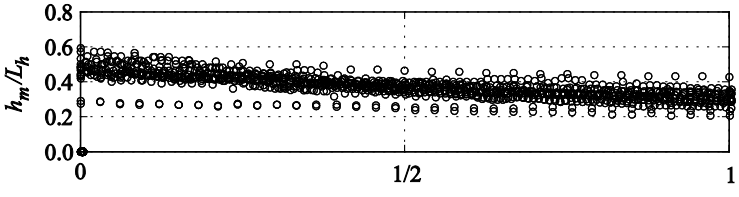

Figure 4 Head aspect ratio as function of the duration of a stretching cycle, for experiment D1.

Similarity between stretching cycles for this variable is clearly observed. The mass growth rate, or stretching rate, of the head can be analyzed by computing the variation of mass during each stretching event over time, i.e., dM_h/dt, herein taken as a measure to assess the entrainment rate at the head. This quantity is thus normalized by the initial mass in the lock, M_0, resulting the parameter $M^* = dM_h/dt\ M_0^{-1}$. Time derivative (dM_h/dt) was computed through application of second order centered finite differences to the experimental data $M_h(t)$, after applying a moving average (N = 10) to instantaneous data.

For comparison between runs, the values of M_h/M_0 (head mass normalized by the initial mass in the lock), and M^*, phase-averaged over one cycle, are shown. Given the different number of points in each

stretching cycle, a sub-discretization of data over one cycle was adopted, taken the shortest temporal discretization within each run, which corresponds to the discretization of the stretching cycle with more data points. Values of variables under analysis are then interpolated linearly in order to have one data point for each additional instant, being then possible to compute phase averages for each run. Figs. 5 to 7 show phase-averaged values over each cycle of variables h_m/L_h, M_h/M_0 and M^*.

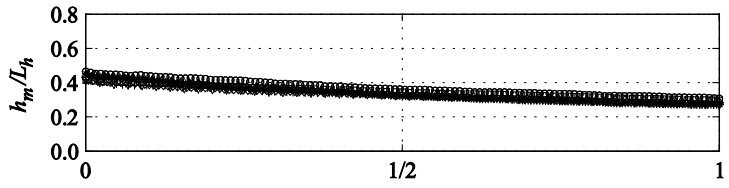

Figure 5 Phase-averaged head aspect ratio as function of the duration of a stretching cycle (symbols explained in Table 1).

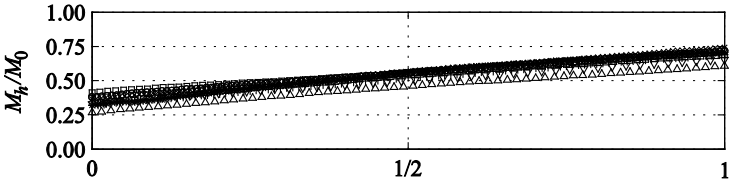

Figure 6 Phase-averaged non-dimensional head mass as function of the duration of a stretching cycle (symbols explained in Table 1).

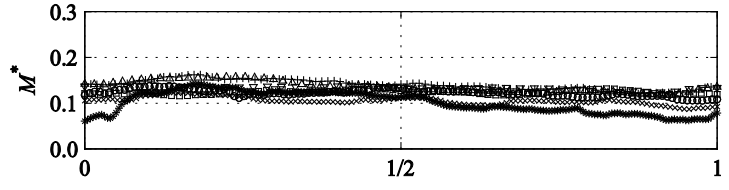

Figure 7 Phase-averaged non-dimensional mass growth rate, as function of the duration of a stretching cycle, (symbols explained in Table 1).

Figures 5 to 7 show similarity between stretching cycles of the variables under analysis. In average terms, the limit attained by the head aspect ratio, related to the end of the stretching phase/occurrence of break event, is around $h_m/L_h \approx 0.3$, thus above the value of 0.2 stated earlier, corroborating previous numerical findings. Mean non-dimensional head mass vary in average between $0.25 < M_h/M_0 < 0.75$. The evolution of M^* during stretching is seen to vary little. There is a general slight increase during the first half of the standard stretching duration, followed by a decrease during the second half. Run R3 exhibits this trend as well, although with a higher amplitude than the remaining runs.

4 CONCLUSIONS AND DISCUSSION

An image analysis technique was used to investigate the dynamics of the head of lock-released gravity currents developing over smooth and rough beds. During the gravity current development, mixing between current and the surrounding ambient fluid exists, leading to entrainment of ambient fluid by the current. The interaction between fluids is more dynamic in the head region and a notorious pattern of head stretching and break was herein observed and described. As the head entrains ambient fluid, it increases in dimension and mass until it becomes unstable and consequently breaks. The evolution of the head aspect ratio during the stretching period shows a consistent limit, for all performed runs, of $h_m/L_h = 0.2$,

corresponding to the instants of break. In addition, during these instants the mass of the gravity current head is seen to be of the same order of the mass initially in the lock, about 75% of the latter in average terms. Bed roughness is seen to play an important role in this process. With an increase of roughness, the breaking events become less frequent. Similarity of the stretching events between runs is confirmed by the consistent collapse of the phase-averaged variables at the head, namely head aspect ratio, non-dimensional head mass and head growth rate. Entrainment at the head was assessed by computing the variation of mass during each stretching event over time. The results presented herein indicate that entrainment at the head is present at all stages of the current development, including the early stages, where higher entrainment rates are observed.

ACKNOWLEDGEMENT

This research was supported by the Portuguese Foundation for Science and Technology (FCT) through the research project PTDC/ECM/099752/2008 and the research grant SFRH/BD/48705/2008.

References

Adduce, C., Lombardi, V., Sciortino, G., and Morganti, M. (2009). Roughness effects on gravity currents dynamics. In Proceedings of 33rd IAHR Congress, Vancouver, Canada.

Bombardelli, F. A., Cantero, M. I., García, M. H., and Buscaglia, G. C. (2009). Numerical aspects of the simulation of descontinuous saline underflows: the lock-exchange problem. J. Hydr. Res., 47(6):777 – 789.

Britter, R. E. and Linden, P. F. (1980). The motion of the front of a gravity current travelling down an incline. J. Fluid Mech., 99(3):531 – 543.

Hacker, J., Linden, P. F., and Dalziel, S. B. (1996). Mixing in lock-release gravity currents. Dynamics of Atmospheres and Oceans, 24:183 – 195.

Hallworth, M. A., Huppert, H. E., Phillips, J. C., and Sparks, R. S. J. (1996). Entrainment into twodimensional and axisymmetric turbulent gravity currents. J. Fluid Mech., 308:289 – 311.

Härtel, C., Meiburg, E., and Necker, F. (2000). Analysis and direct numerical simulation of the flow at a gravity-current head. part 1. flow topology and front speed for slip and no-slip boundaries. J. Fluid Mech., 418:189 – 212.

Kestin, J., Khalifa, H. E., and Correia, R. J. (1981). Tables of the dynamic and kinematic viscosity of aqueous NaCl solutions in the temperature range 20-150c and the pressure range 0.1-35mpa. Physical and Chemical Reference Data, 10(1):71 – 87.

La Rocca, M., Adduce, C., Sciortino, G., and Pinzon, A. B. (2008). Experimental and numerical simulation of three-dimensional gravity currents on smooth and rough bottom. Physics of Fluids, 20.

Marino, B. M., Thomas, L. P., and Linden, P. F. (2005). The front condition for gravity currents. J. Fluid Mech., 536:49 – 78.

Nogueira, H. I. S., Adduce, C., Alves, E., and Franca, M. J. (2012). Dynamics of the head of gravity currents. 4th IAHR International Symposium on Hydraulic Structures, 9-11 February 2012, Porto, Portugal.

Nogueira, H. I. S., Adduce, C., Alves, E., and Franca, M. J. (2013a). Image analysis technique applied to lock-exchange gravity currents. Meas. Sci. Technol. 24 047001.

Nogueira, H. I. S., Adduce, C., Alves, E., and Franca, M. J. (2013b). Analysis of lock-exchange gravity currents over smooth and rough beds. Manuscript accepted for publication in J. Hydr. Res.

Ooi, S. K., Constantinescu, G., and Weber, L. J. (2007). 2D large-eddy simulation of lock exchange gravity current flows at high grashof numbers. J. Hydr. Eng., 133(9):1037 – 1047.

Özgökmen, T.M., Fischer, P. F., Duan, J., and Iliescu, T. (2004). Three-dimensional turbulent bottomdensity currents from a high-order nonhydrostatic spectral element model. J. Physical Oceanogr., 34:2006 – 2026.

Paik, J., Eghbalzadeh, A., and Sotiropoulos, F. (2009). Three-dimensional unsteady rans modelling of discontinuous gravity currents in rectangular domains. J. Hydr. Eng., 135(6):505 – 521.

Rottman, J. W. and Simpson, J. E. (1983). Gravity currents produced by instantaneous releases of a heavy fluid in a rectangular channel. J. Fluid Mech., 135:95 – 110.

Simpson, J. E. (1997). Gravity currents: in the environment and the laboratory. Cambridge University Press, New York, 2nd edition.